JVI Journals.ASM.org

Isolation and Analysis of Rare Norovirus Recombinants from Coinfected Mice Using Drop-Based Microfluidics

Huidan Zhang,[a,b] Shelley K. Cockrell,[c] Abimbola O. Kolawole,[d] Assaf Rotem,[a] Adrian W. R. Serohijos,[e] Connie B. Chang,[a,f] Ye Tao,[a,g] Thomas S. Mehoke,[h] Yulong Han,[a] Jeffrey S. Lin,[h] Nicholas S. Giacobbi,[c] Andrew B. Feldman,[h] Eugene Shakhnovich,[e] David A. Weitz,[a,i] Christiane E. Wobus,[d] James M. Pipas[c]

School of Engineering and Applied Sciences, Harvard University, Cambridge, Massachusetts, USA[a]; Department of Cell Biology, Key Laboratory of Cell Biology, Ministry of Public Health, and Key Laboratory of Medical Cell Biology, Ministry of Education, China Medical University, Shenyang, China[b]; Department of Biological Sciences, University of Pittsburgh, Pittsburgh, Pennsylvania, USA[c]; Department of Microbiology and Immunology, University of Michigan, Ann Arbor, Michigan, USA[d]; Department of Chemistry and Chemical Biology, Harvard University, Cambridge, Massachusetts, USA[e]; Chemical and Biological Engineering Department, Montana State University, Bozeman, Montana, USA[f]; School of Mechatronics Engineering, Harbin Institute of Technology, Harbin, China[g]; Applied Physics Laboratory, Johns Hopkins University, Laurel, Maryland, USA[h]; Department of Physics, Harvard University, Cambridge, Massachusetts, USA[i]

ABSTRACT

Human noroviruses (HuNoVs) are positive-sense RNA viruses that can cause severe, highly infectious gastroenteritis. HuNoV outbreaks are frequently associated with recombination between circulating strains. Strain genotyping and phylogenetic analyses show that noroviruses often recombine in a highly conserved region near the junction of the viral polyprotein (open reading frame 1 [ORF1]) and capsid (ORF2) genes and occasionally within the RNA-dependent RNA polymerase (RdRP) gene. Although genotyping methods are useful for tracking changes in circulating viral populations, they report only the dominant recombinant strains and do not elucidate the frequency or range of recombination events. Furthermore, the relatively low frequency of recombination in RNA viruses has limited studies to cell culture or *in vitro* systems, which do not reflect the complexities and selective pressures present in an infected organism. Using two murine norovirus (MNV) strains to model coinfection, we developed a microfluidic platform to amplify, detect, and recover individual recombinants following *in vitro* and *in vivo* coinfection. One-step reverse transcriptase PCR (RT-PCR) was performed in picoliter drops with primers that identified the wild-type and recombinant progenies and scanned for recombination breakpoints at ~1-kb intervals. We detected recombination between MNV strains at multiple loci spanning the viral protease, RdRP, and capsid ORFs and isolated individual recombinant RNA genomes that were present at a frequency of 1/300,000 or higher. This study is the first to examine norovirus recombination following coinfection of an animal and suggests that the exchange of RNA among viral genomes in an infected host occurs in multiple locations and is an important driver of genetic diversity.

IMPORTANCE

RNA viruses increase diversity and escape host immune barriers by genomic recombination. Studies using a number of viral systems indicate that recombination occurs via template switching by the virus-encoded RNA-dependent RNA polymerase (RdRP). However, factors that govern the frequency and positions of recombination in an infected organism remain largely unknown. This work leverages advances in the applied physics of drop-based microfluidics to isolate and sequence rare recombinants arising from the coinfection of mice with two distinct strains of murine norovirus. This study is the first to detect and analyze norovirus recombination in an animal model.

Recombination contributes to viral diversity and emergence through the exchange of large portions of genetic material (1). Viruses with segmented RNA genomes, such as influenza virus, are shuffled and reassorted to create new virus subspecies (2). Viruses with linear RNA genomes also recombine, but the mechanism is less clear. Current evidence supports a copy choice mechanism in which viral polymerases, including RNA-dependent RNA polymerase (RdRP) and reverse transcriptase (RT), move between coinfecting viral RNAs (1, 3, 4). Several factors have limited our knowledge of the molecular mechanisms and constraints that govern nonsegmented RNA virus recombination and of the biological and public health consequences of viral recombinants. Among these factors are the low frequency of recombination among RNA viruses and the generation of artificial recombinants during PCR and sequencing steps used to detect these rare events (5, 6). Finally, nearly all studies of viral recombination have been limited to *in vitro* or cell culture systems that cannot address the complexities and selective pressures of coinfection in the natural host.

Noroviruses consist of a nonenveloped capsid and a nonseg-

Received 5 May 2015 **Accepted** 10 May 2015

Accepted manuscript posted online 13 May 2015

Citation Zhang H, Cockrell SK, Kolawole AO, Rotem A, Serohijos AWR, Chang CB, Tao Y, Mehoke TS, Han Y, Lin JS, Giacobbi NS, Feldman AB, Shakhnovich E, Weitz DA, Wobus CE, Pipas JM. 2015. Isolation and analysis of rare norovirus recombinants from coinfected mice using drop-based microfluidics. J Virol 89:7722–7734. doi:10.1128/JVI.01137-15.

Editor: S. R. Ross

Address correspondence to James M. Pipas, pipas@pitt.edu.

H.Z. and S.K.C. contributed equally to this work.

doi:10.1128/JVI.01137-15

mented, positive-strand RNA genome of ~7.5 kb (7). Human noroviruses (HuNoVs) are highly abundant viruses that cause sporadic and epidemic gastroenteritis, and outbreaks are often associated with new or recurrent recombination events between circulating strains (8–12). Because human noroviruses have long been recalcitrant to *in vitro* culture (13, 14) and a robust culture system is still being developed (15), murine norovirus (MNV), a closely related virus that replicates in murine macrophages, dendritic cells, and B cells (15, 16), was established as a model system (17). Furthermore, MNV reverse-genetics systems are available to aid mechanistic studies (18, 19). Norovirus recombination has been detected by phylogenetic studies, melt-curve analysis or hybridization of strain-specific probes (20, 21), and full-genome sequencing (21–24). While these methods are useful for tracking recombination in circulating viral populations, they do not reveal the molecular and biological constraints that govern the emergence of particular recombinant strains.

Drop-based microfluidics provides a powerful platform for the high-throughput detection and analysis of rare molecular events, including recombination (25–28). In this system, reaction vessels consisting of picoliter-sized monodispersed drops serve as test tubes for PCRs that are designed to specifically amplify single templates of interest. We recently developed a microfluidic platform to amplify individual recombinants using one-step RT-PCR and to isolate them using fluorescence-activated drop sorting followed by Sanger sequencing (Y. Tao, A. Rotem, H. Zhang, S. K. Cockrell, S. Koehler, C. B. Chang, W. L. Ung, J. S. Lin, A. B. Feldman, C. E. Wobus, J. M. Pipas, and D. A. Weitz, submitted for publication). Because each drop contains a single RNA molecule, the probability of generating artificial chimeras is greatly reduced. Here, we used this strategy to detect rare recombinants generated during coinfections of mice and to reveal novel types of norovirus recombinants. Thus, drop-based microfluidics offers a powerful new approach for the analysis of rare genetic events, including recombination.

MATERIALS AND METHODS

Viruses and cells. The plaque-purified MNV-1 (GV/MNV1/2002/USA) clone MNV-1.CW3 (29) (referred to here as MNV-1) was used at passage 6 for all experiments. MNV-1 and MNV-1 strain WU20 (GenBank accession number EU004665) were propagated in murine macrophage cells (RAW264.7; ATCC) in Dulbecco's modified Eagle's medium (DMEM) supplemented with 10% fetal bovine serum (FBS), 1% HEPES, 1% nonessential amino acids, and penicillin-streptomycin. RAW264.7 cells were plated into 12-well dishes at 2×10^5 cells per well and mock infected or infected with MNV-1 (multiplicity of infection [MOI] of 5), WU20 (MOI of 5), or MNV-1 and WU20 combined (each at an MOI of 2.5). A 1:1 ratio of coinfection was chosen based on a previously reported study (21) and based on the similar infectivity and replication rates of the two parental strains (29). At 24 h postinfection (hpi), infected-cell lysates were freeze-thawed twice and centrifuged at low speed to pellet cell debris. Clarified lysates were stored at −80°C. Viral RNA was prepared with a viral RNA purification kit (Qiagen).

Differential PCR. cDNA was generated from 500 ng RNA with Superscript II RT (Invitrogen) and random hexamer primers. After treatment with RNase H, 0.5 μl cDNA was used for each PCR with Accuprime *Taq* high-fidelity DNA polymerase (Invitrogen) and the PCR primers listed in Table 1, in a total volume of 50 μl. The PCR primers were designed based on the reference sequences for MNV-1 and WU20 (GenBank accession numbers AY228235 and EU004665, respectively) such that each primer oligonucleotide contained 4 to 5 mismatched base pairs between strains and the adjacent PCR products overlapped by 20 to 25 bp. The PCR conditions were 94°C for 1 min; 30 cycles of 94°C for 30 s, *T* (optimal annealing temperature [57.5°C to 63°C] for each primer set) for 30 s, and 68°C for 90 s; and 68°C for 1 min. PCR products were purified by using a PCR purification kit (Qiagen) and run on 0.8% agarose gels. PCR products were excised from agarose and purified with the gel extraction kit (Qiagen). PCR products were sequenced with the primers listed in Table 2. Compared to their reference genomes (GenBank accession numbers AY228235 and EU004665), a few nucleotide substitutions were found in the laboratory strain of MNV-1: G1053A, G2151A, C3809U, C5487U, and A5941G. In WU20, the laboratory strain substitutions included U112A, U2532C, A4865G, and G6173A. This is expected during *in vitro* passaging (18).

cDNA cloning and sequencing. PCR products were TOPO cloned into the pCR2.1 vector (Invitrogen) and transformed into *Escherichia coli* TOP10 cells (Invitrogen). Clones were selected on ampicillin-containing agar and expanded in LB liquid medium with ampicillin. Plasmid minipreps were prepared by the alkaline lysis method, and nucleic acid pellets were resuspended in distilled water (dH_2O) with RNase A. Plasmids were digested with BamHI or HindIII to confirm the insertion of the norovirus PCR product. Selected clones were sequenced (GeneWiz) with universal primers M13R and M13F(−21) in the plasmid vector and the norovirus-specific primers listed in Table 2. The sequencing oligonucleotides were the same for both strains.

Bioinformatics and statistics. Sequence similarity plots were generated with the Simplot program (http://sray.med.som.jhmi.edu/SCRoftware/simplot/) (30). Sequencing alignments used for primer design and TOPO clone analysis were produced with MacVector v.12.0.3. To analyze sequence similarity, protein domain similarity, and GC content in recombination sites, we applied a moving window of 10 nucleotides (nt) over the WU20 genome. The sequence similarity score for each site was the number of mismatches between the WU20 genome and the MNV-1 genome in the next 10 nucleotides. The GC content score for each site was the number of cytosines and guanines among the next 10 nucleotides of the WU20 genome. To analyze protein domain similarity, each of the putative hybrid protein domains created by recombination at a specific mismatch site was compared to both the MNV-1 and WU20 domains. The protein domain similarity score was the smallest mismatch between the hybrid domain and either of the genomes, as a fraction of the maximum possible mismatches in each domain. We compared the distributions of each of the three scores described above in the detected recombination junctions with their distributions over the nondetected recombination junctions using a Kolmogorov-Smirnov test. RNA secondary structures (stems, loops, and junctions) were predicted by Mfold, using default settings (31).

Fabrication of microfluidic devices. Polydimethylsiloxane (PDMS) microfluidic devices were fabricated by using standard soft lithographic methods (32). Two different devices were designed and fabricated: a microfluidic drop maker for encapsulating single recombinant templates in drops and a microfluidic sorter for detecting and sorting fluorescently bright drops. In the PDMS sorting device, electrodes were designed as channels (33). We pushed a low-melting-point metal alloy (Indium Corp.) into the punched holes on an 80°C hot plate and made electrical connections using eight-pin terminal blocks (Phoenix Contact). Finally, the microfluidic channel walls were made hydrophobic by treatment with Aquapel (Pittsburgh Plate Glass, Inc.).

Drop-based one-step RT-PCR. To characterize rare recombinants, we encapsulated and amplified single viral recombinants in drops and then counted, isolated, and sequenced the target amplicons in individual drops. The loading of single viral templates in drops is required to avoid artificial recombination (PCR or RT-PCR chimera), which cannot be distinguished from the true recombinant viral genomes. We assume that viral genomes are suspended homogenously in the purified viral RNA solution, meaning that the loading of suspended viral genomes into drops is determined solely by the concentration of genomes in the suspension: if the genomes are diluted enough in the suspension, then only a small

TABLE 1 Primers used for differential PCR

PCR amplicon	Locus (nt)	Primer	Oligonucleotide sequence[a]
A	1–512	Common-1	GTGAAATGAGGATGGCAACGCCATC
		MNV1-511rc	GCAGCACTGGGGTTGTTGACCC
		WU20-511rc	GCGGCGCCAGGATTGTTGACAC
B	491–1625	MNV1-491	GGTCAACAACCCCAGTGCTGCG
		MNV1-1625rc	GTCGACATCAGCGCGTGGTATGA
		WU20-491	**T**GTCAACAA**T**CC**TGGC**GCC**G**C
		WU20-1625rc	ATCCACGTCGGCACGTGGTATGA
C	1603–2324	MNV1-1603	TCATACCACGCGCTGATGTCGAC
		MNV1-2324rc	GCTCACATTATAGGTGGCACCATTGTAG
		WU20-1603	TCATACCAC**G**T**G**CC**G**GA**C**GT**G**GA**T**
		WU20-2324rc	GCTGACATTGTAGGTAGCCCCGTTGTAG
D	2297–3803	MNV1-2297	CTACAATGGTGCCACCTATAATGTGAGC
		MNV1-3803rc	GACTGCATCAAGGATTTCTTGAGGGG
		WU20-2297	CTACAA**C**GG**G**GC**T**ACCTA**C**AATGT**C**AGC
		WU20-3803rc	AACCGCGTCTAGGATCTCCTGGGGA
E	3778–4724	MNV1-3778	CCCCTCAAGAAATCCTTGATGCAGTC
		MNV1-4724rc	ACGGCGCAGGAAGGAGATGCC
		WU20-3779	**T**CCC**C**AG**G**A**GA**TCCT**A**GA**C**GC**G**GT**T**
		WU20-4724rc	GCGACGCAGAAAGGAAATCCCCT
F	4700–5904	MNV1-4700	GCAGGGCATCTCCTTCCTGCGC
		MNV1-5904rc	ACCGGAGATTGGGGTGGTACCAAGC
		WU20-4701	CAGGG**G**AT**T**TCCTT**T**CTGCG**T**CG**C**
		WU20-5904rc	GCCAGACACAGGTGTCGTGCCAAG
G	5880–6270	MNV1-5880	*TGTAAAACGACGGCCAGT*GCTTGGTACCACCCCAATCTCCGGT
		MNV1-6270rc	CAGGAAACAGCTATGACGATGGTGTCCTGAAAACCGTAGATGG
		WU20-5882	*TGTAAAACGACGGCCAGT*TTGG**C**AC**G**AC**A**CC**TGTG**TC**T**GG**C**
		WU20-6270rc	CAGGAAACAGCTATGACGAGCACATCCTGAAAGAAATAGACAGAGC
H	6245–6522	MNV1-6245	*TGTAAAACGACGGCCAGT*CCATCTACGGTTTTCAGGACACCATC
		MNV1-6521rc	CAGGAAACAGCTATGACCACTCGAACAGCAGTTGCCCAGTCAG
		WU20-6245	*TGTAAAACGACGGCCAGT*C**TG**TCTA**TTTC**TTT-CAGGA**TGTGC**TCCCAG
		WU20-6519rc	CAGGAAACAGCTATGACCTCAAACAGGAGCTGGCCGGTCAA
I	6497–7382	MNV1-6497	TGACTGGGCAACTGCTGTTCGAGTG
		WU20-6494	**T**TGAC**C**GG**C**CA**G**CT**C**CTGTTT**T**GAG
		MNV1-7382rc	AAAATGCATCTAACTACCACAAAGAAAAGAAAGC
		WU20-7382rc	AAAATGCATCTAAATACTACTAAGAAAGAAAAGCAG

[a] Boldface type indicates nucleotide substitutions from MNV-1 to WU20. Italic type indicates universal primer M13F(−21). Underlining indicates universal primer M13R. rc, reverse complement.

number of genomes will be coencapsulated in the same drop, and the chance for chimera generation is negligible (34). Thus, to avoid chimeras and to calculate the relative fraction of recombinant genomes in the sample, we first determined the concentration of viral genomes in our sample. We then diluted the sample to 1 genome per drop to avoid chimeras and determine the concentration of recombinants in the sample. Both reactions were performed by using in-drop one-step RT-PCR. To render successful amplification in drops for their counting and sorting, we added a fluorescent marker to the cocktail. We used one in-drop RT-PCR protocol to determine the total concentration of viral genomes and a second protocol to measure the concentration of recombinant viral genomes.

To measure the concentration of all viral genomes in the sample, the oligonucleotides used to amplify and detect a conserved fragment (nt 39 to 177) for both MNV-1 and WU20 were 5′-CGGGCTGAGCTTCCTG C-3′ (forward primer), 5′-GTGCGCAACACAGAGAAACG-3′ (reverse primer), and 5′-FAM (6-carboxyfluorescein)-CTAGTGTCTCCTTTGG AGCACCTA-3′-TAMRA (6-carboxytetramethylrhodamine) (TaqMan probe) (35). The final volume of the RT-PCR mixture for the amplification of conserved fragments was 25 μl, containing 1 μl of Qiagen OneStep RT-PCR enzyme mix, 1× RT-PCR buffer, 400 μM deoxynucleoside triphosphates (dNTPs), 0.25 μM universal forward and reverse primers, 0.24 μM TaqMan probe, 0.2 μg/μl bovine serum albumin (BSA), 0.5 μl 10% Tween 20, and 1 μl of viral RNA at an unknown concentration. A vacuum system was used to encapsulate the RT-PCR mix into 8-pl aqueous drops dispersed in fluorinated oil containing a surfactant (Tao et al., submitted). The resulting emulsion was thermocycled as follows: 50°C for 30 min; 95°C for 10 min; 40 cycles of 95°C for 30 s, 58°C for 50 s, and 72°C for 1 min; and a final extension step at 72°C for 5 min.

The primers used to detect recombinants are listed in Table 1. The 25-μl RT-PCR mixture for the amplification of recombinant fragments

TABLE 2 Sequencing primers

PCR product/ plasmid insert	Location of priming (nt)	Oligonucleotide sequence
D	2691rc	CTCCTCATCCGTGAGCCCAC
	2406	AAGGAGGCCCGCCTCCGC
	2670	CGTGGGCTCACGGATGAGGAGT
	3418rc	ACATAGGGACAGCCACAGTC
	3636rc	CAGAACATGGTCTTGGTGCTC
	3399	GACTGTGGCTGTCCCTATGT
E	4129rc	GCGCGAATCATGGTGCCAAG
	3921	CAGAAGAGCAAGGACTGGAC
	4111	TTGGCACCATGATTCGCGC
	4335	CCTCTCCCCTGAGCCAGACT
F	5080rc	GCGCTGCGCCATCACTCA
	4881	GAGGCTGCCATGCATGGTG
	5509rc	CACATCACACATGACATGTGGGA
	5202	CCAAATTGACCCCTGGATCTTC
	5485	TCCCACATGTCATGTGTGATGTG

rc, reverse complement.

contained 0.5 μl SuperScript III RT/Platinum *Taq* high-fidelity enzyme mix (Invitrogen), 1× reaction buffer, 0.2 μM universal forward and reverse primers, 0.08× EvaGreen, 0.2 μg/μl BSA, 0.5 μl 10% Tween 20, and 1 μl viral RNA. After determining the concentration of total RNA in the first reaction mixture, we diluted the sample in the second reaction mixture to 1 parental virus per 8-pl drop, equivalent to 12.8 pg/μl of RNA. The conditions for recombinant fragment amplification were as follows: 55°C for 30 min; 94°C for 2 min; 40 cycles of 95°C for 15 s, 60°C for 30 s, and 68°C for 90 s; and a final extension step at 68°C for 5 min.

Detection, isolation, and sequencing of viral templates with recombinant fragments. A microfluidic fluorescent drop sorter was used to detect and isolate drops containing recombinant amplicons (see Fig. 3A). Drops containing amplified templates had significantly higher levels of fluorescence than did those not containing the amplified template, enabling their detection as bright drops. The concentration of viral RNA was calculated by counting the bright drops, each representing the amplification of a single genome. Bright drops were sorted and distributed into 96-well plates with at most 1 template per well. The contents of each sorted drop were reamplified by using a 25-μl PCR mixture that contained 0.5 μl KAPAHiFi DNA polymerase, 1× KAPAHiFi buffer, 200 μM dNTPs, 0.2 μM forward and reverse primers, and 5 μl of the template. The sample was thermocycled as follows: 95°C for 3 min; 35 cycles of 98°C for 20 s, 60°C for 15 s, and 72°C for 90 s; and a final extension step at 72°C for 5 min. The PCR products were purified with a GenElute gel extraction kit (Sigma) and Sanger sequenced (Tao et al., submitted).

***In vivo* coinfection studies.** Mouse studies were performed in accordance with local and federal guidelines outlined in the *Guide for the Care and Use of Laboratory Animals* of the National Institutes of Health (36). Protocols were approved by the University of Michigan Committee on Use and Care of Animals (UCUCA) (approval number 09710). Four- to eight-week-old STAT1$^{-/-}$ mice (strain 2045) were purchased from Taconic Farms Inc. and housed at the University of Michigan animal care facility, where all experiments were conducted. Mice were infected orally (p.o.) or intraperitoneally (i.p.) with 10^6 PFU of each virus for a total of 2×10^6 PFU when combined. Mice were housed individually on metal grates, and all of the shed feces were removed every 24 h. Three days after infection, mice were humanely euthanized according to the approved protocol. The mesentery, spleen, and liver were harvested. Samples were homogenized as described previously (37), and virus titers were determined by a plaque assay (38).

Nucleotide sequence accession numbers. The laboratory strain MNV-1 and WU20 sequences were deposited in GenBank under accession numbers KM102450 and KM102449, respectively.

RESULTS

Norovirus recombination occurs at multiple locations on the viral genome. Genotyping assays have demonstrated recombination between norovirus strains at the open reading frame 1 (ORF1)/ORF2 junction or in selected regions within ORF1 (20–22, 39). To determine whether recombination can occur in other regions of the genome, a scan across the entire viral genome for potential sites of recombination was performed. To that end, a differential PCR method was designed, which amplified the entire genomes of murine norovirus strains MNV-1 and WU20 in 9 reactions, generating amplicons A to I (Fig. 1A). The MNV-1 and WU20 strains were used because their 87% nucleotide sequence identity (21) suggests a high probability of recombination (40) and because recombination has been shown to occur between them (21). Comparative genomic analysis of the two parental genomes revealed 9 segments that are bounded by regions of the genome where MNV-1 and WU20 are <80% identical, allowing us to target each segment with strain-specific primers (Table 1). For each segment, four primer sets were used: MNV-1-forward and MNV-1-reverse (primer set 1 [p1]), WU20-forward and WU20-reverse (p2), MNV-1-forward and WU20-reverse (p3), and WU20-forward and MNV-1-reverse (p4) (Fig. 1B). p1 and p2

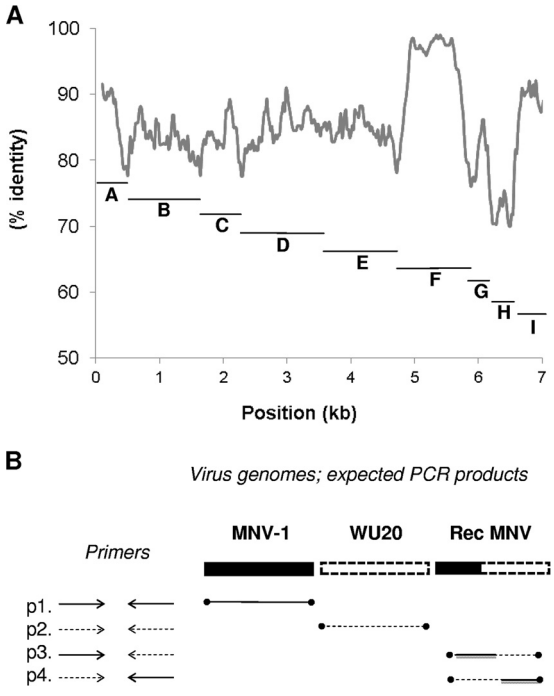

FIG 1 Differential PCR detects recombination between norovirus strains. (A) Similarity plot of MNV-1 and WU20 (gray trace) with a diagram of the expected PCR products (amplicons A to I [black bars]) (see also Table 1). The *x* axis indicates the position on the viral genome (in kilobases). The *y* axis indicates the similarity score at each nucleotide position. (B) Primer pair design. For each PCR product, four primer sets were used: p1 (MNV-1-forward and MNV-1-reverse), p2 (WU20-forward and WU20-reverse), p3 (MNV-1-forward and WU20-reverse), and p4 (WU20-forward and MNV-1-reverse). Primer sets 1 and 2 anneal to parental strains only (MNV-1 or WU20), while primer sets 3 and 4 detect recombinants (Rec MNV).

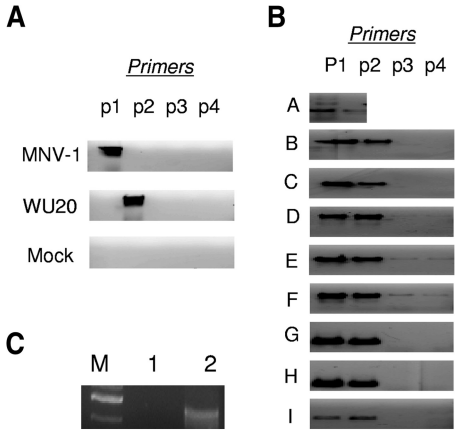

FIG 2 Validation of differential PCR. (A) Efficiency and specificity of p1 to p4. p1 and p2 specifically amplify MNV-1 and WU20, respectively, while p3 and p4 did not generate PCR products from parental strain cDNA. Mock indicates no viral template input. (B) The full panel of RT-PCR products (amplicons A to I) representing the parental strains MNV-1 (p1) and WU20 (p2) as well as recombinants (p3 and p4) in viral RNA purified from RAW264.7 cells coinfected with MNV-1 and WU20. (C) Differential PCR products analyzed by drop-based digital PCR. Mixed MNV-1 and WU20 RNA (lane 1) or RNA from RAW264.7 cells coinfected with MNV-1 and WU20 (lane 2) was encapsulated in drops with p4 and subjected to RT-PCR. The 1,200-bp recombinant product was amplified only from RNA purified from coinfected cells. M, molecular size markers (top, 1,500 bp; bottom, 1,000 bp).

were expected to anneal to parental strains only, while p3 and p4 amplify PCR products only if recombination between the two strains occurred. Each PCR was optimized to ensure that no product was generated when strain-specific primers were used with cDNA from the mismatched viral genome (Fig. 2A). This assay could not be used to detect recombination at the extreme 5′ end of the genome (bp 1 to 64), as the similarity between the strains was too great to design differential primers. By using the full panel of PCR products, the complete genomes of both strains were sequenced and were found to match their corresponding references. These data demonstrate that two closely related MNV strains, MNV-1 and WU20, can be distinguished by differential PCR, which laid the foundation for the identification of recombination events.

To assay recombination between strains, murine macrophage (RAW264.7) cells were coinfected with MNV-1 and WU20. RNA from cell lysates was harvested and reverse transcribed to cDNA, which was used in differential PCRs. For each genomic fragment generated by PCR, the parental MNV-1 and WU20 sequences were prominent (Fig. 2B, lanes 1 and 2, amplicons A to I). Faint bands of recombinant products were observed in amplicons D, E, and F with primer sets p3 and p4 (Fig. 2B, lanes 3 and 4), suggesting that there were recombinant fragments corresponding to bp 2297 to 5904 of the MNV genome (i.e., the coding region of the C terminus of NS4 [3A-like] to the N-terminal half of VP1). No recombinant PCR products were generated with primers external to this region (Fig. 2B, lanes 3 and 4, amplicons B, C, and G to I).

To control for potential artifacts introduced during reverse transcription and PCR, cDNA prepared from mock-infected and singly MNV-1- and WU20-infected RAW264.7 cells as well as cDNA prepared from total and RNase-protected RNA isolated from coinfected cells were used as the templates for differential PCR (Fig. 3A). To ensure that reverse transcription and PCR did not introduce false-positive recombinants, RNAs or cDNAs from singly infected cells were mixed (1:1) prior to RT or PCR, respectively; these mixed templates showed no evidence of recombination, demonstrating the specificity of the reaction. In contrast, when cDNA was prepared from both total and RNase-protected RNAs from coinfected cells, amplicons were generated by p3 and p4 within amplicons D, E, and F (bp 2297 to 3803, 3778 to 4724, and 4700 to 5904, respectively), suggesting that recombinant genomes were generated and successfully packaged into nascent viral capsids.

To determine the loci of recombination between MNV-1 and WU20, the recombinant PCR products D3, D4, E3, E4, F3, and F4 were sequenced. The initial Sanger sequencing reads had many overlapping and ambiguous base calls (data not shown), suggesting that multiple recombinants with different recombination breakpoints were present. To identify the individual recombination breakpoints, the F-region PCR products were ligated into a TOPO-pCR2.1 vector, and plasmid clones were Sanger sequenced. Overlapping reads were assembled into contigs, which were aligned with the MNV-1 and WU20 reference sequences. As previously reported (21), some recombination events were observed in the ORF1/2 junction between the RdRP and capsid genes (Fig. 3B). However, we also observed recombination breakpoints within ORF2 in the region encoding the S domain of the capsid protein. Taken together, these data suggest that recombinant genomes are being generated and can be detected by differential PCR.

Detection of recombination events by using drop-based microfluidics. Two caveats of using differential PCR to detect recombinants, however, are the generation of chimera artifacts resulting from false priming or strand switching during amplification (41, 42) and the lack of a quantitative measure for the frequency of recombination. To overcome these problems, we utilized RT-PCR in drops (Tao et al., submitted). Specifically, we developed a microfluidic device to dilute individual genomes into 8.25-pl-drop PCR chambers for RT-PCR (Fig. 4A). The drops were ~25 μm in size, which ensured their stability during thermocycling and high downstream sorting rates. Each drop contained a DNA-intercalating dye, EvaGreen, which was used to detect the successful production of PCR amplicons. Total MNV genomes were diluted in the premixed RT-PCR reagents so that no more than one genome copy was encapsulated in each drop. After thermocycling, the drops were transferred to a fluorescent drop sorting device, which detects and counts fluorescent drops while also deflecting them into a positive sorting channel. Each captured drop was then transferred into one well of a 96 well-plate, where the drops were disrupted to allow reamplification of the genomic material. The second-round PCR products were then Sanger sequenced.

To quantify the frequency of recombination events during *in vitro* coinfection, we split the total RNA isolated from the MNV-1/WU20-coinfected cell lysate and measured the concentration of total virus templates by RT-PCR in drops using the primer pairs for a conserved fragment in ORF1 (nt 39 to 177). To determine the number of recombinant genomes, the same RNA sample was examined by RT-PCR in drops by using p4 for the F region. The estimated frequency of recombinant viruses in the coinfected sample was 1/2,500, well above the chance for chimeras, which is on the order of 1/10,000,000 for the dilution factor of viral templates that we used (Tao et al., submitted). To confirm the ampli-

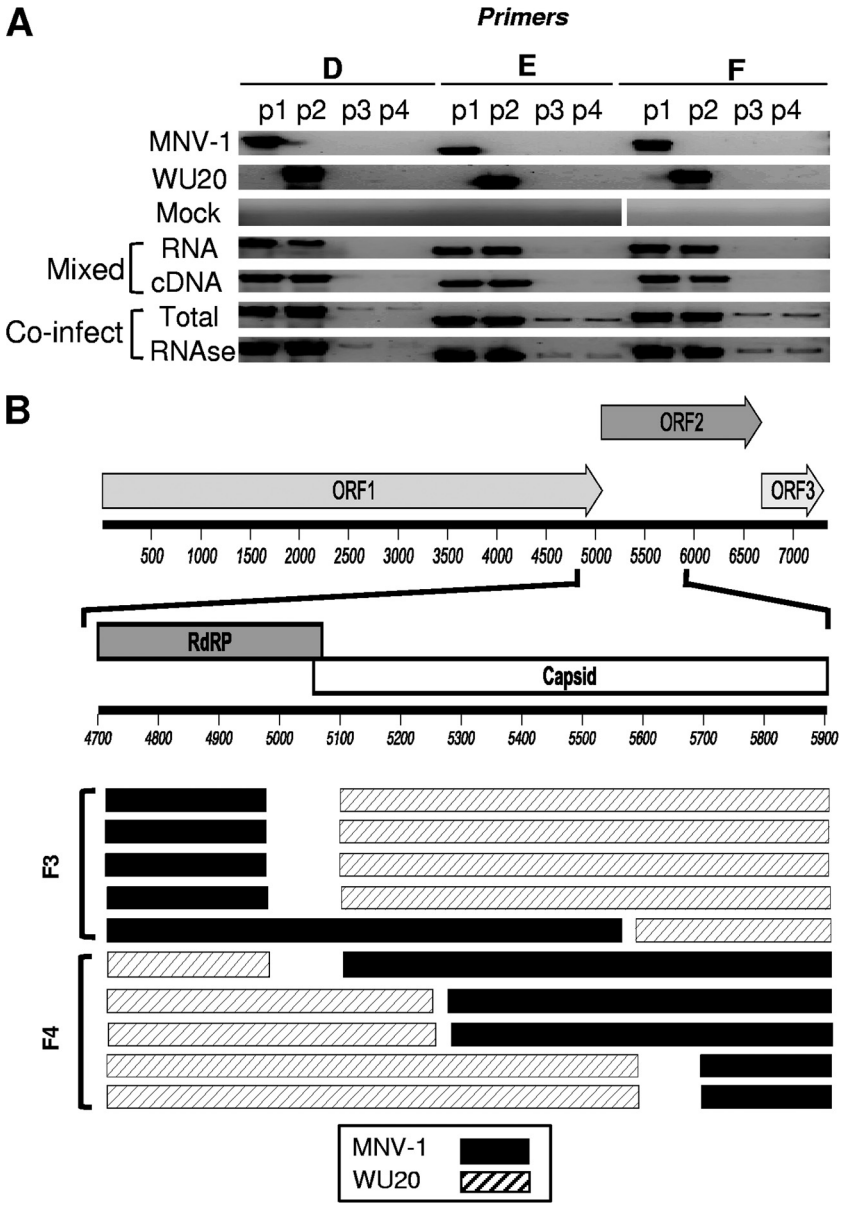

FIG 3 Detection of recombination events in cells coinfected with MNV-1 and WU20. (A) Differential PCR of viral cDNA from *in vitro* coinfections. By using the primer pair combinations outlined in Fig. 1B, differential PCR for amplicons D to F was performed on samples of cells singly infected with MNV-1 or WU20, the mock lysate (top three panels), mixed RNA and cDNA from singly infected cells (middle two panels), and total or RNase-treated samples following coinfection (bottom two panels). (B, top) Recombination events detected in the region encompassing nt 4700 to 5904, a region that spans the ORF1/2 junction. The PCR products generated from total RNA after coinfection and from p3 and p4 (PCR products F3 and F4, respectively) (Fig. 2A, bottom right) were cloned into TOPO vectors. (Bottom) Five individual plasmid clones from each set were sequenced and aligned with the MNV-1 and WU20 reference sequences. Gaps between bars indicate 100% identity between WU20 and MNV-1 sequences.

fication of recombinant RNA templates in drops, we recovered amplicons from the drops and analyzed them by agarose gel electrophoresis. Only RNA prepared from coinfected cultured cells generated the recombinant amplicon band (Fig. 2C). To sequence individual recombinant templates, we sorted and isolated 15 bright drops into 45 wells and reamplified the contents of each well. Nine of the 15 bright drops contained recombinant amplicons (Fig. 4B), while the remaining drops contained nonspecific amplification products and primer dimers, as determined by agarose gel electrophoresis. One of the recombination events detected in drops at the junction between the RdRP and capsid genes was previously reported (21) and was observed in the plasmid clones (nt 5056 to 5069) (first three recombinants in Fig. 4B). We also found six other recombinants within the ORF2/capsid gene that were not observed in the plasmid clones (forth to ninth recombinants in Fig. 4B). These data demonstrate the potential of drop-based microfluidics for detecting and counting viral recombinants.

Isolation of recombinants following coinfection of mice. To determine whether recombinants are also generated between MNV-1 and WU20 *in vivo*, highly susceptible STAT1$^{-/-}$ mice (43) were infected with MNV-1 and WU20 singly (1 mouse each/

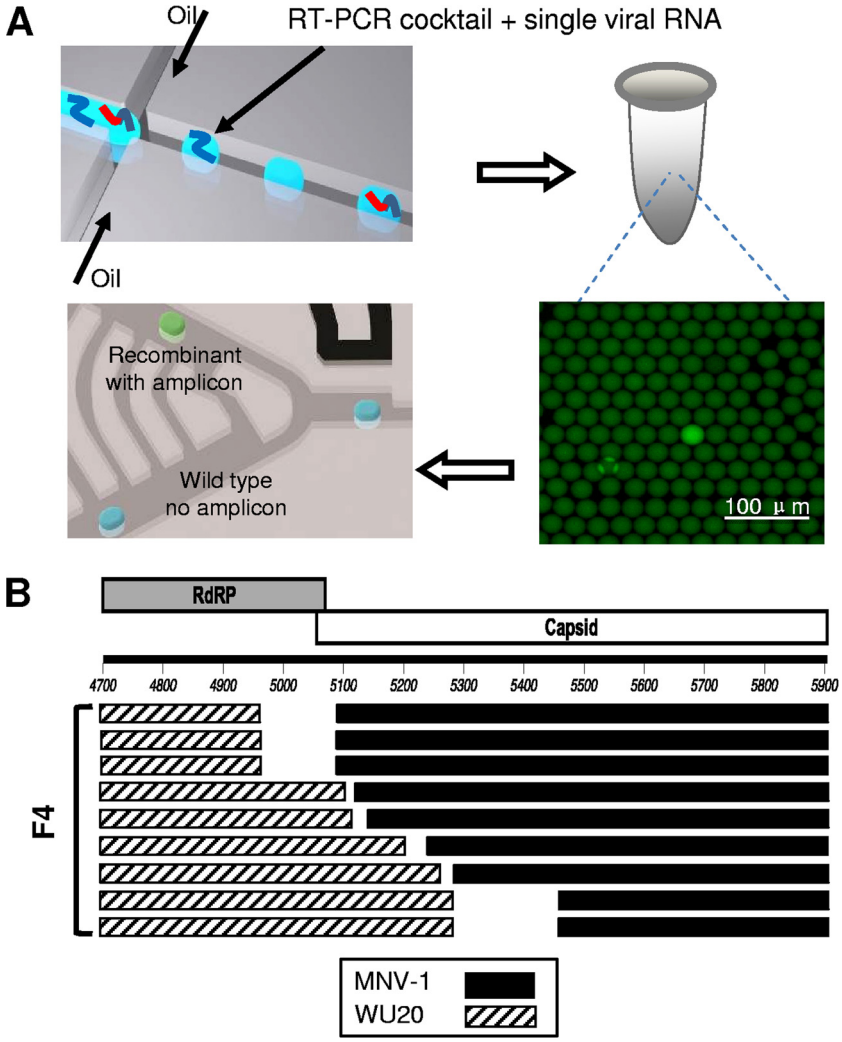

FIG 4 Drop-based microfluidic platform for detecting recombinant MNV. (A) Schematic representation of RT-PCR in drops. (Top left) A one-step RT-PCR mixture with purified viral RNA was encapsulated in monodispersed picoliter drops by using a microfluidic drop maker. Each drop contained no more than one template (blue lines) and specific primers (red lines) for the detection of recombination. (Top right) Drops were collected in a PCR tube and subjected to thermocycling conditions for RT-PCR. (Bottom right) Drops with successfully amplified recombinant sequences generated a fluorescence signal from the DNA-intercalating dye EvaGreen. After thermocycling, drops were examined by fluorescence microscopy. (Bottom left) The thermocycled drops were reinjected into a microfluidic sorter, and drops containing amplicons (green) were detected via laser-induced fluorescence (488 nm) and sorted by dielectrophoresis. (B) Total RNA from *in vitro* coinfections was encapsulated in drops with primers specific for nt 4700 to 5904 (F amplicon; p4 [WU20-forward and MNV-1-reverse]). The contents of 9 drops containing 6 unique recombinants were sequenced and aligned with the MNV-1 and WU20 reference sequences. Gaps between bars indicate 100% identity betweenWU20 and MNV-1.

route) or in combination (3 mice/route). Mice were infected orally to mirror the natural route of infection (44) and intraperitoneally to circumvent the intestinal epithelial barrier, a known bottleneck (45). To prevent reinfection of mice via coprophagy, mice were housed on metal grates, and excreted feces were removed every 24 h. The mesentery, liver, and spleen were harvested at 72 h postinfection (hpi). Viral titers in feces (48 to 72 hpi) and tissues were determined by a plaque assay (Fig. 5A) and droplet quantitative RT-PCR (qRT-PCR) (Fig. 5B). Oral infection produced significantly higher numbers of infectious virions than did intraperitoneal infection in the collected tissues but not in feces, which contained significantly lower viral loads than those in tissues (Fig. 5A). Viral genome copy numbers following oral infection were similar in spleen and mesentery, while fewer viral genomes reached the liver and were excreted in the feces following intraperitoneal infection (Fig. 5B). Overall, genome titers were ~200-fold higher than infectious titers in tissues and ~10^5-fold higher in feces. The former is similar to the PFU/genome ratio observed in cell culture (46).

When attempts were made to detect recombinants from *in vivo* samples by using differential PCR, the target signal proved to be low compared to the sensitivity of amplification. However, additional amplification in bulk risks the generation of chimera artifacts resulting from false priming or strand switching during amplification (41, 42). To avoid these problems, we utilized drop-based RT-PCR and encapsulated samples at diluted concentrations to prevent the formation of chimeras (Tao et al., submitted). We analyzed the total virus genomes using primer pairs for a conserved fragment in ORF1 (nt 39

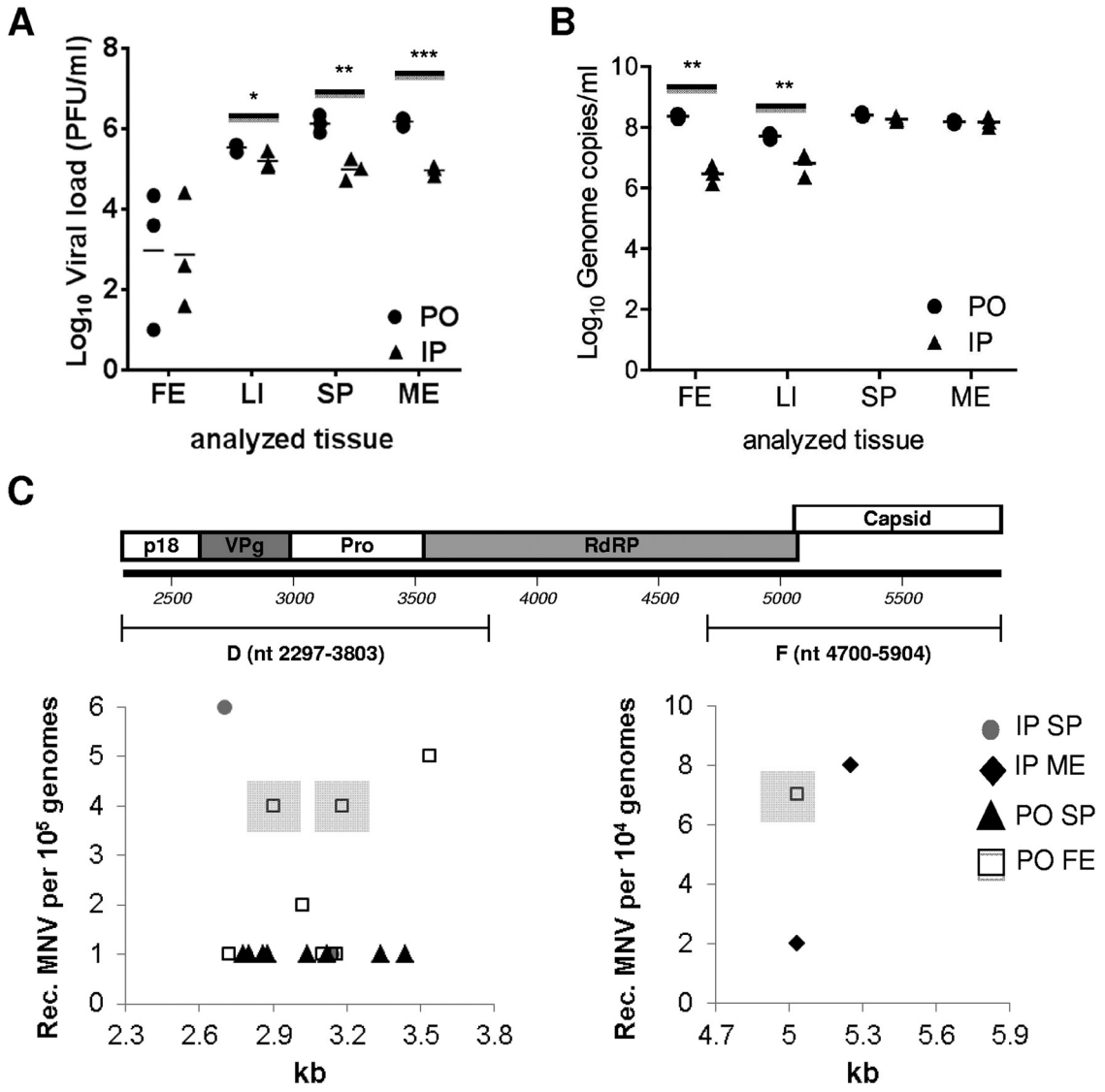

FIG 5 Detection of MNV recombinants from *in vivo* coinfections. Individually housed STAT1$^{-/-}$ mice were infected with MNV-1 and WU20 orally (PO) or intraperitoneally (IP). Feces (FE) were removed every 24 h. The indicated tissues were harvested at 72 hpi. SP, spleen; LI, liver; ME, mesentery. (A) Viral loads in tissues and feces (48 to 72 hpi) were determined by a plaque assay. Each symbol represents one mouse. The mean viral titers for the combined group are indicated by black lines. (B) Genome titers in tissues and feces (48 to 72 hpi) were measured by drop-based RT-PCR. Each symbol represents one mouse. The means are indicated by black lines. *, $P < 0.05$; **, $P < 0.01$; ***, $P < 0.001$ (by Student *t* test). (C, top) Partial MNV genome showing coding regions within amplicons D and F (nt 2297 to 3803 and 4700 to 5904, respectively). (Bottom) Total recombinants in different tissues were counted by drop-based RT-PCR using specific primers. Recombinants were sorted and sequenced to determine the locus of recombination. Identical sites of recombination in different mice are highlighted with gray boxes.

to 177) and for recombinant virus genomes in the regions spanning nt 2297 to 3808 and 4700 to 5904 (amplicons D and F, respectively; amplicon E was not analyzed). In total, we analyzed ~2.4 × 10^6 virus-containing drops from 6 different mice (3 per route) and detected and sequenced 51 recombinant genomes (Fig. 5C and Table 3). Multiple recombinants were detected in various tissues following either intraperitoneal or oral infection (Fig. 5C). As a control, the RNA from feces of mice infected orally with MNV-1 or WU20 alone was mixed and subjected to drop-based RT-PCR with recombination-specific primers (D region, p4); no recombinants were identified in the 147,376 genomes scanned. For the F region, mixed RNA produced no detectable recombinants out of 7,000 scanned viral genomes.

The recombination rate differed greatly depending on the infection route, tissue, and genomic locus, ranging from <0.3 recombinants (no bright drops in 300,000 drops) to 156 recombinants (7 bright drops in 4,500 drops) per 100,000 genomes (Table 3). The mice tested for recombinants in amplicon F (mesentery of one i.p. infected mouse and feces of one p.o. infected mouse) had on average 1 recombinant per 1,000 genomes at two different locations at the ORF1/2 junction: both mice had recombinants at nt 4967 to 5099, a known recombination site (21), and an additional recombinant was detected in the mesentery of the i.p. infected mouse at nt 5238 to 5264. The high frequency of these recombinants, three times higher than the probability of recombination measured *in vitro* (3.3 × 10^{-4}), suggested that these recombinant viruses may be capable of replica-

TABLE 3 Frequency of *in vivo* recombinants measured by microfluidics[a]

Route of infection	Sample type	Mean no. of recombinants/10^5 viruses ± SD	
		Region D	Region F
p.o.	Feces (48–72 hpi)	6.3 ± 1.5[b]	156 ± 59
	Liver	<0.3	ND
	Spleen	2.7 ± 0.9[c]	ND
	Mesentery	<0.3	ND
	Feces (48–72 hpi)	<0.3	ND
i.p.	Liver	<0.3	ND
	Spleen	2.3 ± 0.9[d]	ND
	Mesentery	<0.3	63 ± 20

[a] p.o., oral infection; i.p., intraperitoneal infection; ND, not determined.
[b] There were 3 recombinants in mouse 1, 3 in mouse 2, and 13 in mouse 3.
[c] There were no recombinants in mouse 1, 6 in mouse 2, and 2 in mouse 3.
[d] There were 6 recombinants in mouse 1, 0 in mouse 2, and 1 in mouse 3.

tion. In contrast, recombinants in amplicon D were rarer, averaging <4 per 100,000 genomes. Moreover, since the mismatches between parental genomes are more abundant and more evenly spaced in amplicon D than in amplicon F, the distribution of recombinants over all amplicon D loci can be reliably obtained. Interestingly, two of the recombinants in amplicon D were detected multiple times in the same sample: all 6 recombinants in the spleen of one i.p. infected mouse were located at nt 2699 to 2720, near the 5′ end of the VPg gene; 5 of 13 recombinants in the feces of one p.o. infected mouse were located at nt 3533 to 3539, near the 5′ end of the RdRP; and all 3 recombinants in the feces of another p.o. infected mouse were located at nt 3174 to 3176 in the protease coding region. The probability that these recombinants will cooccur by chance is $<10^{-8}$, suggesting a bias of recombination toward these regions. Finally, multiple identical recombinants were detected in the feces of different mice at nt 2883 to 2921 near the 3′ end of the VPg coding region (two p.o. infected mice) and at nt 3174 to 3176 in the protease coding region (two p.o. infected mice). These data demonstrate that drop-based microfluidics can be used to detect rare recombinant MNV genomes *in vivo* and highlight the variety of recombination loci generated *in vivo*.

Influence of protein sequence, RNA sequence, and structure on recombination. To determine molecular parameters that govern viral recombination, we compared the detected loci of recombination with the background of all potential mismatches between the two viral genomes and searched for a significant overrepresentation of properties in one group versus the other. We focused our search on the properties associated with RNA sequence, RNA structure, and protein structure. To study the bias of recombination toward regions that cooccurred significantly more frequently than by chance in our samples, we analyzed the sporadically occurring recombinants (Fig. 6A and B, green bars) separately from the cooccurring recombinants (Fig. 6A and B, blue bars).

First, we tested the influence of protein structure on determining the recombination sites. Previous work using protein engineering showed that recombinants with splice points in the middle of the protein tend to be less functional than those with splice points close to the N or C termini (47). For each potential recombination site in the genome, we calculated the number of amino acids that will mismatch between the putative recombinant protein and the most similar parental protein: sites that are closer to a protein boundary will incur fewer mismatches in the hybrid protein, and the probability that they are functional is higher. Recombinants that were detected sporadically in amplicon D *in vivo* are not located closer to domain boundaries than the putative hybrids (Fig. 6A). Interestingly, the recombinants detected in amplicons D and F that cooccur are located closer to domain boundaries than the putative hybrids (Kolmogorov-Smirnov *P* values of 0.04 for amplicon D and 3×10^{-5} for amplicon F) (Fig. 6A and B, domain mismatch), suggesting that these recombinants may be capable of replicating.

Next, the recombination sites detected *in vivo* were searched for biases in GC content and sequence similarity because GC content is highly correlated with recombination in higher-order organisms (48), while sequence similarity between the two genomes may favor template switching (49). To test the correlations of GC content and/or sequence similarity within the detected recombination sites in regions D and F, we averaged the two variables over the genome by using a window that extended 10 bp downstream. While the GC contents of both the WU20 and MNV-1 genomes were distributed similarly in the detected recombination sites compared to the background of all mismatch sites (data not shown), the sequence similarity between the WU20 and MNV-1 genomes was significantly higher in the cooccurring recombination sites detected in amplicon D and in the recombination sites detected in amplicon F than in the background of all potential recombination sites (Kolmogorov-Smirnov *P* values of 1.1×10^{-3} for amplicon D and 10^{-20} for amplicon F) (Fig. 6A and B, sequence mismatch). These findings support the notion that template switching between the two parental genomes occurs in regions of high sequence similarity.

RNA structures of the viral genomes can also be an important determinant of viral recombination (49–51). The detected recombination sites are tightly localized in specific regions of the RNA molecule, as shown for one example in Fig. 6C, suggesting that some features of the RNA secondary or tertiary structure affect recombination. One possibility is the transition between loop and stem structures that may stall the RdRP, increasing the chance of template switching in such regions (Fig. 6D). To analyze these features, we examined the predicted secondary structure of the original template genome from which the RdRP is expected to switch. In our case, the original template is WU20, since our primers target template switching from WU20 to MNV-1. We therefore analyzed the secondary structure of the WU20 RNA genome with Mfold (top 25 configurations) and categorized it as loops, stems, and junctions. Analysis was carried out with amplicon D only, since recombination regions in amplicon F are sparse and each of them spans a large portion of the amplicon, which weakens the statistical power of the analysis. Although there was no difference in the fractions of stems, loops, and junctions in the detected recombination sites compared to the rest of amplicon D (data not shown), there was a difference in the proximity to junctions that constitute a transition from loop to stem in the direction of RdRP activity (i.e., 5′ to 3′): the detected sites of recombination were on average only 1.3 ± 0.05 nt away from a loop-to-stem junction, while the rest of the sites were on average 1.8 ± 0.03 nt away from such junctions (Kolmogorov-Smirnov *P* value of 10^{-9}) (Fig. 6E). This difference was consistent over all of the suggested RNA secondary structures. Taken together, these data suggest that MNV recombination *in vivo* may be influenced by RNA secondary structure elements.

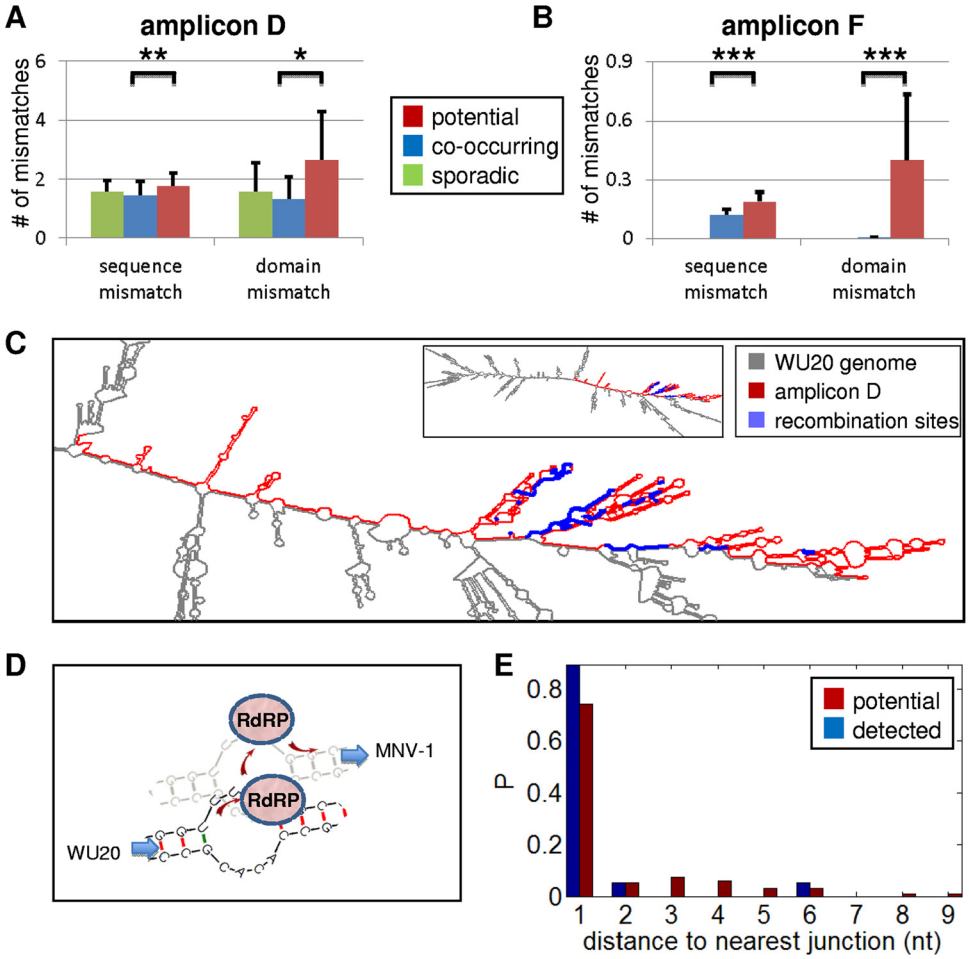

FIG 6 Analysis of recombination site RNA sequences, RNA structure, and protein domains. (A) *In vivo* recombination sites in amplicon D (nt 2297 to 3803) that cooccur in the samples more frequently than by chance (see Result for details) were biased toward sequence similarity (two-sample Kolmogorov-Smirnov *P* value of 1.1×10^{-3}) and toward protein domain similarity (two-sample Kolmogorov-Smirnov *P* value of 0.04). Recombination sites that occurred sporadically in amplicon D were not biased toward sequence or protein domain similarity. Here sequence mismatch is the number of nucleotides mismatching in a 10-bp window and domain mismatch is the distance to the nearest domain boundary in mismatching amino acids (see Materials and Methods). A *P* value of <0.05 rejects the null hypothesis that the two samples were drawn from the same continuous distribution. (B) *In vivo* recombination in amplicon F (nt 4700 to 5904) was significantly biased toward both sequence similarity (two-sample Kolmogorov-Smirnov *P* value of 3×10^{-5}) and known protein domain similarity (two-sample Kolmogorov-Smirnov *P* value of 10^{-20}). (C) Localization of detected recombinants in amplicon D in the secondary structure. Detected recombination regions are plotted over the secondary RNA structure of amplicon D and the genome. Recombination sites tended to localize in 3 stem/loop regions of the molecule. This observation was robust across the first 25 configurations proposed by Mfold for the complete WU20 genome (the inset shows the first configuration), suggesting that some features of the RNA secondary or tertiary structure correlate with a higher probability of recombination. (D) Proposed model for recombination. During transcription, the RdRP dwells longer at locations where single-stranded RNA (loop) hybridizes to another strand to become a stem, presumably increasing the potential for template switching at those sites. (E) To test for recombination bias toward loop-to-stem junctions, the distance to the nearest loop-to-stem junction was measured for each recombination site. Detected recombination sites were on average 1.3 ± 0.03 nt away from a loop-to-stem junction, significantly closer than potential recombination sites that were on average 1.8 ± 0.02 nt away from a junction. The data include recombination sites that are 6 nt or shorter; junctions were calculated for 25 different secondary RNA structures.

DISCUSSION

RNA recombination is an important driving force of viral evolution, and understanding the spectrum of potential recombination is critical to understanding viral emergence. We have developed a highly sensitive microfluidics system with digital PCR to detect rare viral genetic recombinants *in vivo*. Recombination resulting from coinfection with two murine norovirus strains, MNV-1 and WU20, was detected in cell culture and in the native host, with recombination sites being located in previously known (e.g., the ORF1/2 junction) and unknown (i.e., VPg/protease) regions of the viral genome. The differential PCR and drop-based screening described here are broadly applicable to any type of virus, enabling future studies of virus evolution in infected organisms.

Our findings were made possible by two technological advances: the development of a differential PCR-based genotyping assay to detect genetic recombination between MNV strains across the entire length of the viral genome and a microfluidic-based digital RT-PCR to detect very rare recombination events. The development of a differential PCR-based genotyping assay was based on a previous study of murine norovirus recombination between MNV-1 and WU20 that iden-

tified one recombinant at the junction of ORF1 and ORF2 by designing primers targeting three previously known recombination regions of the MNV genome (21). By using the same MNV strains, primers were expanded to target the entire MNV genome. To overcome shortfalls (i.e., false-positive results) of differential PCR, we next took advantage of recent developments in the microfluidics field (52) that applied this technology for use in high-throughput biological assays (26, 53–57). The power of microfluidics in biological applications lies in the production of millions of picoliter-sized drops, each of which serves as a single reaction chamber. These very small sample volumes are amenable to high-speed measurements, leading to cost reduction and shortened screening time. After we adapted differential RT-PCR to the drop system, we highly diluted the samples so that each drop contained at most a single template, thus removing the potential of PCR chimeras. The abundance of nonspecific amplification products typical of any large-cycle-number amplification method is easily discarded without losing the true recombinants, by reamplifying the contents of single drops and selecting recombinants by gel electrophoresis (Tao et al., submitted). We screened $\sim 10^8$ drops in $\sim$7 h, making the microfluidics-based RT-PCR technique a method for the detection of very rare recombination events in general.

Our study identified the highest frequency of recombination at the junction of ORF1 and ORF2 in the MNV genome, in agreement with data from previous studies (12, 20, 22). We also detected lower frequencies of MNV recombination in the VPg, protease, and 3′ end of the RdRP coding region as well as the VP1 S domain (Fig. 5). To our knowledge, no natural recombinants in the region of the genome encoding VPg or protease have been described. Previous analyses of naturally isolated MNV strains describe recombination breakpoints in the VP1 P domain and the ORF2/3 junction (29), while some human noroviruses show recombination sites in ORF2 at the junction of the S and P domains and at the ORF2/3 junction (8, 58). However, we did not examine recombination at these sites because no recombinant MNV was detected in culture lysates for amplicons G to I (nt 5880 to 7382). While the findings in this work are fundamental and novel, further data collection and more biological replicates are necessary to precisely determine the frequency of recombination as well as for more in-depth studies of recombination events.

Following the identification of multiple recombinants across the viral genome, we examined the influence of three parameters on norovirus recombination. GC content had no effect on recombination, while recombination junctions occurred more frequently in regions of the two genomes with high sequence similarity. In addition, the local RNA secondary structure appeared to influence the position of recombination junctions, and recombination was more likely to occur in single-stranded loops and was disfavored in stems where the bases are hydrogen bonded to other bases. It may be possible that during transcription, the RdRP dwells longer at locations where single-stranded RNA (loop) hybridizes to another strand to become a stem, increasing the potential for template switching at those sites. (Fig. 6D). A similar propensity for recombination to occur near regions of secondary structure was recently reported for picornaviruses (59).

The significance of recombination is evident in norovirus, as circulating recombinant strains cause pandemics every 2 to 3 years. Recombinant strains of significant public health impact occur in many RNA viruses (40). RNA recombination contributes to viral evolution by allowing the exchange of more substantial genetic material than point mutations, thus causing changes in biological properties, including an increased ability to avoid host immunity or increased viability and fitness (40, 60). Thus, high-throughput genetic screens using microfluidic devices may help detect and predict recombination events that lead to increased virulence in viruses or other pathogens.

ACKNOWLEDGMENTS

This work was supported by Defense Advanced Research Projects Agency (DARPA) grant HR0011-11-C-0093.

We are grateful to Paul Cantalupo and Josh Katz (Department of Biological Sciences, University of Pittsburgh) for assistance with bioinformatic analyses, and we thank other members of the DARPA Prophecy program team for valuable discussions.

REFERENCES

1. **Simon-Loriere E, Holmes EC.** 2011. Why do RNA viruses recombine? Nat Rev Microbiol **9:**617–626. http://dx.doi.org/10.1038/nrmicro2614.
2. **Knipe DM, Howley PM, Cohen JI, Griffin DE, Lamb RA, Martin MA, Racaniello VR, Roizman B (ed).** 2013. Fields virology, 6th ed. Lippincott Williams & Wilkins, Philadelphia, PA.
3. **Kirkegaard K, Baltimore D.** 1986. The mechanism of RNA recombination in poliovirus. Cell **47:**433–443. http://dx.doi.org/10.1016/0092-8674(86)90600-8.
4. **Onafuwa-Nuga A, Telesnitsky A.** 2009. The remarkable frequency of human immunodeficiency virus type 1 genetic recombination. Microbiol Mol Biol Rev **73:**451–480. http://dx.doi.org/10.1128/MMBR.00012-09.
5. **Yu W, Rusterholtz KJ, Krummel AT, Lehman N.** 2006. Detection of high levels of recombination generated during PCR amplification of RNA templates. Biotechniques **40:**499–507. http://dx.doi.org/10.2144/000112124.
6. **Wu L, Tang T, Zhou R, Shi S.** 2007. PCR-mediated recombination of the amplification products of the Hibiscus tiliaceus cytosolic glyceraldehyde-3-phosphate dehydrogenase gene. J Biochem Mol Biol **40:**172–179. http://dx.doi.org/10.5483/BMBRep.2007.40.2.172.
7. **Green KY.** 2007. Caliciviridae, p 949–980. *In* Knipe DM, Howley PM, Griffin DE, Lamb RA, Martin MA, Roizman B, Straus SE (ed), Fields virology, 5th ed, vol 1. Lippincott Williams & Wilkins, Philadelphia, PA.
8. **Lam TT, Zhu H, Smith DK, Guan Y, Holmes EC, Pybus OG.** 2012. The recombinant origin of emerging human norovirus GII.4/2008: intragenotypic exchange of the capsid P2 domain. J Gen Virol **93:**817–822. http://dx.doi.org/10.1099/vir.0.039057-0.
9. **Giammanco GM, Rotolo V, Medici MC, Tummolo F, Bonura F, Chezzi C, Martella V, De Grazia S.** 2012. Recombinant norovirus GII.g/GII.12 gastroenteritis in children. Infect Genet Evol **12:**169–174. http://dx.doi.org/10.1016/j.meegid.2011.10.021.
10. **Vega E, Vinje J.** 2011. Novel GII.12 norovirus strain, United States, 2009-2010. Emerg Infect Dis **17:**1516–1518. http://dx.doi.org/10.3201/eid1708.110025.
11. **Mathijs E, Denayer S, Palmeira L, Botteldoorn N, Scipioni A, Vanderplasschen A, Thiry E, Dierick K.** 2011. Novel norovirus recombinants and of GII.4 sub-lineages associated with outbreaks between 2006 and 2010 in Belgium. Virol J **8:**310. http://dx.doi.org/10.1186/1743-422X-8-310.
12. **Mahar JE, Kirkwood CD.** 2011. Characterization of norovirus strains in Australian children from 2006 to 2008: prevalence of recombinant strains. J Med Virol **83:**2213–2219. http://dx.doi.org/10.1002/jmv.22215.
13. **Lay MK, Atmar RL, Guix S, Bharadwaj U, He H, Neill FH, Sastry KJ, Yao Q, Estes MK.** 2010. Norwalk virus does not replicate in human macrophages or dendritic cells derived from the peripheral blood of susceptible humans. Virology **406:**1–11. http://dx.doi.org/10.1016/j.virol.2010.07.001.
14. **Duizer E, Schwab KJ, Neill FH, Atmar RL, Koopmans MP, Estes MK.** 2004. Laboratory efforts to cultivate noroviruses. J Gen Virol **85:**79–87. http://dx.doi.org/10.1099/vir.0.19478-0.
15. **Jones MK, Watanabe M, Zhu S, Graves CL, Keyes LR, Grau KR, Gonzalez-Hernandez MB, Iovine NM, Wobus CE, Vinje J, Tibbetts SA, Wallet SM, Karst SM.** 2014. Enteric bacteria promote human and mouse

norovirus infection of B cells. Science **346:**755–759. http://dx.doi.org/10.1126/science.1257147.
16. **Wobus CE, Karst SM, Thackray LB, Chang KO, Sosnovtsev SV, Belliot G, Krug A, Mackenzie JM, Green KY, Virgin HW.** 2004. Replication of norovirus in cell culture reveals a tropism for dendritic cells and macrophages. PLoS Biol **2:**e432. http://dx.doi.org/10.1371/journal.pbio.0020432.
17. **Wobus CE, Thackray LB, Virgin HW, IV.** 2006. Murine norovirus: a model system to study norovirus biology and pathogenesis. J Virol **80:**5104–5112. http://dx.doi.org/10.1128/JVI.02346-05.
18. **Arias A, Bailey D, Chaudhry Y, Goodfellow I.** 2012. Development of a reverse-genetics system for murine norovirus 3: long-term persistence occurs in the caecum and colon. J Gen Virol **93:**1432–1441. http://dx.doi.org/10.1099/vir.0.042176-0.
19. **Ward VK, McCormick CJ, Clarke IN, Salim O, Wobus CE, Thackray LB, Virgin HW, IV, Lambden PR.** 2007. Recovery of infectious murine norovirus using pol II-driven expression of full-length cDNA. Proc Natl Acad Sci U S A **104:**11050–11055. http://dx.doi.org/10.1073/pnas.0700336104.
20. **Bull RA, Hansman GS, Clancy LE, Tanaka MM, Rawlinson WD, White PA.** 2005. Norovirus recombination in ORF1/ORF2 overlap. Emerg Infect Dis **11:**1079–1085. http://dx.doi.org/10.3201/eid1107.041273.
21. **Mathijs E, Muylkens B, Mauroy A, Ziant D, Delwiche T, Thiry E.** 2010. Experimental evidence of recombination in murine noroviruses. J Gen Virol **91:**2723–2733. http://dx.doi.org/10.1099/vir.0.024109-0.
22. **Bull RA, Tanaka MM, White PA.** 2007. Norovirus recombination. J Gen Virol **88:**3347–3359. http://dx.doi.org/10.1099/vir.0.83321-0.
23. **Ren XW, Yang F, Hu YF, Zhang T, Liu LG, Dong J, Sun LL, Zhu YF, Xiao Y, Li L, Yang J, Wang JW, Jin Q.** 2013. Full genome of influenza A (H7N9) virus derived by direct sequencing without culture. Emerg Infect Dis **19:**1881–1884. http://dx.doi.org/10.3201/eid1911.130664.
24. **Wong TH, Dearlove BL, Hedge J, Giess AP, Piazza P, Trebes A, Paul J, Smit E, Smith EG, Sutton JK, Wilcox MH, Dingle KE, Peto TE, Crook DW, Wilson DJ, Wyllie DH.** 2013. Whole genome sequencing and de novo assembly identifies Sydney-like variant noroviruses and recombinants during the winter 2012/2013 outbreak in England. Virol J **10:**335. http://dx.doi.org/10.1186/1743-422X-10-335.
25. **Agresti JJ, Antipov E, Abate AR, Ahn K, Rowat AC, Baret JC, Marquez M, Klibanov AM, Griffiths AD, Weitz DA.** 2010. Ultrahigh-throughput screening in drop-based microfluidics for directed evolution. Proc Natl Acad Sci U S A **107:**4004–4009. http://dx.doi.org/10.1073/pnas.0910781107. (Author Correction, 107:6550, http://dx.doi.org/10.1073/pnas.1002891107.)
26. **Guo MT, Rotem A, Heyman JA, Weitz DA.** 2012. Droplet microfluidics for high-throughput biological assays. Lab Chip **12:**2146–2155. http://dx.doi.org/10.1039/c2lc21147e.
27. **Hayden RT, Gu Z, Ingersoll J, Abdul-Ali D, Shi L, Pounds S, Caliendo AM.** 2013. Comparison of droplet digital PCR to real-time PCR for quantitative detection of cytomegalovirus. J Clin Microbiol **51:**540–546. http://dx.doi.org/10.1128/JCM.02620-12.
28. **Pekin D, Skhiri Y, Baret JC, Le Corre D, Mazutis L, Ben Salem C, Millot F, El Harrak A, Hutchison JB, Larson JW, Link DR, Laurent-Puig P, Griffiths AD, Taly V.** 2011. Quantitative and sensitive detection of rare mutations using droplet-based microfluidics. Lab Chip **11:**2156–2166. http://dx.doi.org/10.1039/c1lc20128j.
29. **Thackray LB, Wobus CE, Chachu KA, Liu B, Alegre ER, Henderson KS, Kelley ST, Virgin HW, IV.** 2007. Murine noroviruses comprising a single genogroup exhibit biological diversity despite limited sequence divergence. J Virol **81:**10460–10473. http://dx.doi.org/10.1128/JVI.00783-07.
30. **Lole KS, Bollinger RC, Paranjape RS, Gadkari D, Kulkarni SS, Novak NG, Ingersoll R, Sheppard HW, Ray SC.** 1999. Full-length human immunodeficiency virus type 1 genomes from subtype C-infected seroconverters in India, with evidence of intersubtype recombination. J Virol **73:**152–160.
31. **Zuker M.** 2003. Mfold Web server for nucleic acid folding and hybridization prediction. Nucleic Acids Res **31:**3406–3415. http://dx.doi.org/10.1093/nar/gkg595.
32. **McDonald JC, Duffy DC, Anderson JR, Chiu DT, Wu HK, Schueller OJA, Whitesides GM.** 2000. Fabrication of microfluidic systems in poly(dimethylsiloxane). Electrophoresis **21:**27–40. http://dx.doi.org/10.1002/(SICI)1522-2683(20000101)21:1<27::AID-ELPS27>3.0.CO;2-C.
33. **Siegel AC, Shevkoplyas SS, Weibel DB, Bruzewicz DA, Martinez AW, Whitesides GM.** 2006. Cofabrication of electromagnets and microfluidic systems in poly(dimethylsiloxane). Angew Chem Int Ed Engl **45:**6877–6882. http://dx.doi.org/10.1002/anie.200602273.
34. Reference deleted.
35. **Taube S, Perry JW, Yetming K, Patel SP, Auble H, Shu L, Nawar HF, Lee CH, Connell TD, Shayman JA, Wobus CE.** 2009. Ganglioside-linked terminal sialic acid moieties on murine macrophages function as attachment receptors for murine noroviruses. J Virol **83:**4092–4101. http://dx.doi.org/10.1128/JVI.02245-08.
36. **National Research Council.** 2011. Guide for the care and use of laboratory animals, 8th ed. National Academies Press, Washington, DC.
37. **Kolawole AO, Li M, Xia C, Fischer AE, Giacobbi NS, Rippinger CM, Proescher JB, Wu SK, Bessling SL, Gamez M, Yu C, Zhang R, Mehoke TS, Pipas JM, Wolfe JT, Lin JS, Feldman AB, Smith TJ, Wobus CE.** 2014. Flexibility in surface-exposed loops in a virus capsid mediates escape from antibody neutralization. J Virol **88:**4543–4557. http://dx.doi.org/10.1128/JVI.03685-13.
38. **Gonzalez-Hernandez MB, Bragazzi Cunha J, Wobus CE.** 2012. Plaque assay for murine norovirus. J Vis Exp **2012:**e4297. http://dx.doi.org/10.3791/4297.
39. **Waters A, Coughlan S, Hall WW.** 2007. Characterisation of a novel recombination event in the norovirus polymerase gene. Virology **363:**11–14. http://dx.doi.org/10.1016/j.virol.2007.03.012.
40. **Galli A, Bukh J.** 2014. Comparative analysis of the molecular mechanisms of recombination in hepatitis C virus. Trends Microbiol **22:**354–364. http://dx.doi.org/10.1016/j.tim.2014.02.005.
41. **Judo MS, Wedel AB, Wilson C.** 1998. Stimulation and suppression of PCR-mediated recombination. Nucleic Acids Res **26:**1819–1825. http://dx.doi.org/10.1093/nar/26.7.1819.
42. **Kanagawa T.** 2003. Bias and artifacts in multitemplate polymerase chain reactions (PCR). J Biosci Bioeng **96:**317–323. http://dx.doi.org/10.1016/S1389-1723(03)90130-7.
43. **Karst SM, Wobus CE, Lay M, Davidson J, Virgin HW, IV.** 2003. STAT1-dependent innate immunity to a Norwalk-like virus. Science **299:**1575–1578. http://dx.doi.org/10.1126/science.1077905.
44. **Green KY.** 2013. Caliciviridae: the noroviruses, p 582–608. *In* Knipe DM, Howley PM, Cohen JI, Griffin DE, Lamb RA, Martin MA, Racaniello VR, Roizman B (ed), Fields virology, 6th ed, vol 1. Lippincott Williams & Wilkins, Philadelphia, PA.
45. **Kuss SK, Etheredge CA, Pfeiffer JK.** 2008. Multiple host barriers restrict poliovirus trafficking in mice. PLoS Pathog **4:**e1000082. http://dx.doi.org/10.1371/journal.ppat.1000082.
46. **Baert L, Wobus CE, Van Coillie E, Thackray LB, Debevere J, Uyttendaele M.** 2008. Detection of murine norovirus 1 by using plaque assay, transfection assay, and real-time reverse transcription-PCR before and after heat exposure. Appl Environ Microbiol **74:**543–546. http://dx.doi.org/10.1128/AEM.01039-07.
47. **Drummond DA, Silberg JJ, Meyer MM, Wilke CO, Arnold FH.** 2005. On the conservative nature of intragenic recombination. Proc Natl Acad Sci U S A **102:**5380–5385. http://dx.doi.org/10.1073/pnas.0500729102.
48. **Marsolier-Kergoat MC, Yeramian E.** 2009. GC content and recombination: reassessing the causal effects for the Saccharomyces cerevisiae genome. Genetics **183:**31–38. http://dx.doi.org/10.1534/genetics.109.105049.
49. **Draghici HK, Varrelmann M.** 2010. Evidence for similarity-assisted recombination and predicted stem-loop structure determinant in potato virus X RNA recombination. J Gen Virol **91:**552–562. http://dx.doi.org/10.1099/vir.0.014712-0.
50. **Mikkelsen JG, Lund AH, Duch M, Pedersen FS.** 1998. Recombination in the 5′ leader of murine leukemia virus is accurate and influenced by sequence identity with a strong bias toward the kissing-loop dimerization region. J Virol **72:**6967–6978.
51. **Simon-Loriere E, Martin DP, Weeks KM, Negroni M.** 2010. RNA structures facilitate recombination-mediated gene swapping in HIV-1. J Virol **84:**12675–12682. http://dx.doi.org/10.1128/JVI.01302-10.
52. **Livak-Dahl E, Sinn I, Burns M.** 2011. Microfluidic chemical analysis systems. Annu Rev Chem Biomol Eng **2:**325–353. http://dx.doi.org/10.1146/annurev-chembioeng-061010-114215.
53. **Zagnoni M, Cooper JM.** 2011. Droplet microfluidics for high-throughput analysis of cells and particles. Methods Cell Biol **102:**25–48. http://dx.doi.org/10.1016/B978-0-12-374912-3.00002-X.
54. **Mary P, Chen A, Chen I, Abate AR, Weitz DA.** 2011. On-chip background noise reduction for cell-based assays in droplets. Lab Chip **11:**2066–2070. http://dx.doi.org/10.1039/c1lc20159j.
55. **Chang CM, Chang WH, Wang CH, Wang JH, Mai JD, Lee GB.** 2013.

Nucleic acid amplification using microfluidic systems. Lab Chip **13:**1225–1242. http://dx.doi.org/10.1039/c3lc41097h.

56. **Bogojevic D, Chamberlain MD, Barbulovic-Nad I, Wheeler AR.** 2012. A digital microfluidic method for multiplexed cell-based apoptosis assays. Lab Chip **12:**627–634. http://dx.doi.org/10.1039/C2LC20893H.
57. **Fischer AE, Wu SK, Proescher JB, Rotem A, Chang CB, Zhang H, Tao Y, Mehoke TS, Thielen PM, Kolawole AO, Smith TJ, Wobus CE, Weitz DA, Lin JS, Feldman AB, Wolfe JT.** 2015. A high-throughput drop microfluidic system for virus culture and analysis. J Virol Methods **213:**111–117. http://dx.doi.org/10.1016/j.jviromet.2014.12.003.
58. **Eden JS, Tanaka MM, Boni MF, Rawlinson WD, White PA.** 2013. Recombination within the pandemic norovirus GII.4 lineage. J Virol **87:**6270–6282. http://dx.doi.org/10.1128/JVI.03464-12.
59. **Runckel C, Westesson O, Andino R, DeRisi JL.** 2013. Identification and manipulation of the molecular determinants influencing poliovirus recombination. PLoS Pathog **9:**e1003164. http://dx.doi.org/10.1371/journal.ppat.1003164.
60. **Austermann-Busch S, Becher P.** 2012. RNA structural elements determine frequency and sites of nonhomologous recombination in an animal plus-strand RNA virus. J Virol **86:**7393–7402. http://dx.doi.org/10.1128/JVI.00864-12.